

A novel insight into vertical ground motion modelling in earthquake engineering

L.P. ARGANI^{1,2} AND A. GAJO¹

¹*Department of Civil, Environmental & Mechanical Engineering, University of Trento, via Mesiano 77, I-38123 Trento, Italy*

²*Department of Mathematical Sciences, University of Liverpool, Mathematical Sciences Building, Liverpool L69 7ZL, UK*

Abstract

Recent observations of failure and damage of buildings and structures under seismic action has led to an increasing interest for an in-depth analysis of the vertical component of site ground motion. In particular, when dealing with saturated soils, the current engineering practice does not usually go beyond the simplified $u-p$ formulation of the Biot's equations describing the coupled hydro-mechanical behaviour, thus neglecting some terms of fluid inertial forces, despite the presence of more refined formulations, e.g. the $u-U$ formulation. Therefore, a theoretical and numerical validation of the $u-p$ formulation as compared with the $u-U$ formulation is proposed in this work, where the numerical simulations are compared with the analytical solution for the $u-p$ formulation, which is also derived and illustrated in this text. The comparison between the two formulations and the analytical solution is provided for different levels of permeability and dynamic actions, which are representative of a wide scenario of site ground properties and seismic hazard in the vertical direction. In particular, the soil response is analysed in terms of acceleration and pore pressure time history, frequency content, acceleration response spectrum, and amplification ratio of acceleration. This study extends the discussion of the limits of applicability of the $u-p$ formulation with respect to the rigorous solution of Biot's equations (obtained here with $u-U$ formulation) to the context of a complex dynamic regime provided by the vertical components of real earthquake records, and paves the way for further investigations.

Keywords: soil dynamics, vertical ground motion, earthquake engineering, analytical solution, finite element modelling, $u-p$ and $u-U$ formulation

1 Introduction

In Geotechnical and Structural Engineering there is an increasing interest in the analysis of the vertical component of site ground motion. In fact, it is well known that damages to buildings, structures, and bridges during an earthquake may arise from the horizontal component as well as from the vertical component of site ground motion. It is noted that a limited emphasis is given to the vertical component on earthquake ground motion by the current seismic design regulations, as the horizontal component is usually considered

to be more relevant. A number of seismic protection systems that are developed for the design of special constructions (i.e. petrochemical plants and storage systems [1, 2]) are mainly focused on the effects of the horizontal component of seismic actions, despite these constructions may undergo detrimental effects when subjected the vertical component of the seismic actions. However, different real earthquakes showed that the vertical to horizontal peak ground acceleration ratio can be above unity [3–7], denoting that this feature can play an important role in seismic design [8]. This situation typically occurs within few dozen kilometres from a seismic source, in the so-called near-field or epicentral area where, depending on fault dimension and rupture mechanism, specific ground motion effects can occur [9–12]. Since the pioneering work by Housner & Trifunac [9] it has been recognised that in the near-field domain engineering structures can be exposed to seismic demands that are much different from those arising from far-field domain, which correspond to the typical demands that influence the design of the structures, both in terms of intensity and, especially, of nature of ground motion [13]. The vertical component of ground motion typically focuses its energy in a high frequency band (commonly above 5 Hz [13]) and, within 5 km from the source, the peaks of vertical and horizontal components can be considered to occur almost simultaneously [4, 14, 15]. This is a typical condition for the Apennine region, where historical towns are located on or very close to active faults, as occurred in L’Aquila (2009, Italy) earthquake [16].

Nevertheless, the effects of the vertical component of site ground motion are rarely investigated in detail and only simplified formulations are usually employed in the current practice when performing finite element modelling, whereas several tools are available for the horizontal component. In particular, the coupled hydro-mechanical behaviour of saturated soils under static and dynamic conditions can be described by means of the Biot’s equations [17, 18], for which different formulations are proposed in literature [19–21]. There is a constant interest in developing refined numerical formulations addressed to include the full set of Biot’s equations also in the context of large strains [22–24]; however, the modelling of saturated soils under static and dynamic conditions is commonly performed by means of the well known u - p formulation of the Biot’s equations; an alternative choice is the u - U formulation [19, 25], which is rarely employed in engineering practice due to its much higher computational costs, and the same holds for u - w , u - w - p , and u - U - p formulations, although they are capable to describe the response when pore fluid accelerations are not negligible with respect to those of the solid phase. In particular, the u - w - p formulation leads to a proper Lagrangian formulation for the solid skeleton and a completely Eulerian formulation for the fluid in terms of pore pressure p and relative velocity w with respect to the solid skeleton (and hence reveals to be suitable also to describe quasi-static situations involving filtration), whereas the u - U - p formulation allows to take into account for absolute pore water displacement U . Further investigations on these refined formulations can be found, for instance, in recent works that are devoted to the implementation of the u - w - p formulation [23, 26] and of the u - U - p formulation [27] at large strain.

Despite being widely employed, the u - p formulation is based on a set of simplifications that limit its range of validity in terms of maximum frequency content of input motions, of thickness, and of permeability of the soil layers [28]. In particular, Zienkiewicz *et al.* [29] indicate that the acceleration frequencies are low in the case of earthquake motions, so that the terms in the governing equations involving the relative acceleration of the fluid become negligible. Furthermore, the current formulation of such validity limits is limited

to the linear elastic response and considers only longitudinal wave propagation.

The aim of this work is to present a novel theoretical validation of the widely diffused $u-p$ formulation as compared to the $u-U$ formulation of the Biot's equations for the analysis of the vertical component of site ground motion in the dynamic regime. The proposed validation is intended as an extension of the validation proposed by Zienkiewicz *et al.* [28] and is based on two sets of case studies: (i) the propagation of a single longitudinal pulse in a laboratory sample; (ii) the seismic response of a soil layer subjected to a set of registered vertical seismic ground motions applied at the soil base. This validation is performed within the elastic response of the soil, as it was performed by Zienkiewicz *et al.* [28]. Although the non-linear behaviour of soil (e.g. soil plasticity) is of paramount importance to accurately describe the soil response, soil plasticity is not taken into account in this work in order to avoid any possible dependency of the results on the chosen constitutive model, and the focus is on the basic features of the $u-p$ formulation. On the other hand, it is expected that the effects of the elastic-plastic response of the soil can lead to increased differences between the behaviour predicted by two formulations. In fact, a difference in the pore pressure evaluation by means of the two formulations can lead to a difference in the effective stress computation, which, in turn, can lead to a different non-linear behaviour as the constitutive modelling depends on the (mean) effective stress itself.

Although a combination of the vertical component of both S waves, surface waves and P waves can trigger the vertical ground motion acting on a structure, the case studies are devoted to the modelling of the sole P waves in the near-field in order to provide a clear interpretation of the results. Due to this assumption, this study is limited to the one-dimensional modelling of the soil.

It is also important to remark that the validation of Zienkiewicz *et al.* [28] is based on a single frequency soil motion applied at the the top surface of a soil layer, and their validation was limited to the error on pore pressure. The results of the case studies proposed in this work allow to extend the validation of Zienkiewicz *et al.* [28] to the general case of seismic ground motions encompassing an interval of frequencies. In this work, the validation is extended to the computed frequencies content, acceleration response spectrum, and amplification ratio of acceleration. In particular, it is shown that in the case of a wide frequency range ground motion, the graphical representation of the validity ranges proposed by Zienkiewicz *et al.* [28] for a single frequency ground motion should be treated with caution and should be accompanied with a thorough analysis of the errors in the acceleration and pore pressure time history, the frequencies content, the acceleration response spectrum and amplification, in order to define the appropriate limits of applicability of the the $u-p$ formulation.

To this purpose, the analytical solution of the $u-p$ formulation is derived and compared with the numerical results obtained with the $u-p$ formulation implemented as a user-defined subroutine in a commercial finite element code (Abaqus Unified FEA®) and with those obtained with the $u-U$ formulation implemented in an in-house finite element code [30]. In particular, a parametric study is performed in order to investigate the vertical site response as a function of the soil permeability, the soil layer thickness and the soil state conditions. The results and the comparisons are provided in terms of the frequency content, the type of the seismic site ground motion, and the amplification function. Finally, the limits of applicability of the $u-p$ as compared to $u-U$ formulations for applications in Geotechnical Earthquake Engineering are discussed.

2 Governing equations

In this section, the governing equations for the u - p formulation and for the u - U formulation of saturated porous media are summarised, together with a brief description of their numerical implementation within a finite element framework. The analytical solution for the longitudinal wave propagation problem is derived for the u - p formulation, which is used as a benchmark for the first case study (discussed in section 3.1). It is worth recalling that the u - U numerical results were validated by using the analytical solution proposed by Gajo & Mongiovì [31].

2.1 u - p formulation and analytical solution

The well known u - p formulation for the dynamic behaviour of saturated porous media is obtained by neglecting the inertial forces of the pore fluid related to the relative acceleration of the fluid with respect to the solid and can be expressed by the following set of equations [21, 28] for a linear-elastic soil response (small strain theory is assumed):

$$d\sigma_{ij} = d\sigma''_{ij} - \alpha \delta_{ij} dp, \quad (1a)$$

$$\varepsilon_{ij} = \frac{1}{2} \left(\frac{\partial u_i}{\partial x_j} + \frac{\partial u_j}{\partial x_i} \right), \quad (1b)$$

$$d\sigma''_{ij} = \mathbb{D}_{ijkl} (d\varepsilon_{kl} - d\varepsilon_{kl}^0), \quad (1c)$$

$$\frac{\partial \sigma_{ij}}{\partial x_j} + \rho g_i = \rho \frac{\partial^2 u_i}{\partial t^2}, \quad (1d)$$

$$\alpha \frac{\partial \varepsilon_{ii}}{\partial t} + \frac{K_D}{g} \frac{\partial}{\partial x_i} \left(-\frac{1}{\rho_f} \frac{\partial p}{\partial x_i} + g_i - \frac{\partial^2 u_i}{\partial t^2} \right) + \frac{1}{Q} \frac{\partial p}{\partial t} = 0, \quad (1e)$$

where u_i is the displacement of the solid skeleton, σ_{ij} is the total stress tensor, σ''_{ij} is the Nur & Byerlee [32] effective stress tensor, ε_{ij} is the strain tensor, ε_{kl}^0 is the initial (creep or thermal) strain tensor, \mathbb{D}_{ijkl} is the elastic stiffness tensor, K_D is the Darcy permeability coefficient, ρ is the density of the whole porous medium, ρ_f is the pore fluid density, g_i is i -th component of the gravity acceleration (having modulus g), whereas α is the Biot's coefficient and Q is the bulk modulus of the mixture, which are expressed as

$$\alpha = 1 - \frac{K}{K_s}, \quad (2a)$$

$$\frac{1}{Q} = \frac{n}{K_f} + \frac{\alpha - n}{K_s}, \quad (2b)$$

being n the porosity, while K_s , K_f , and K are the bulk modulus of the solid skeleton, of the pore fluid, and of the mixture, respectively. The density of the whole porous medium can be expressed as

$$\rho = (1 - n)\rho_s + n\rho_f. \quad (3)$$

It can be noted that the fluid mass balance equation (1e) includes inertial forces due to pore fluid. The effects of these forces are discussed in the next section.

When dealing with the problem of longitudinal wave propagation, for instance along the x_1 axis, and assuming null body forces, it is possible to rewrite equations (1d) and (1e)

as:

$$M \frac{\partial^2 u}{\partial x^2} - \alpha \frac{\partial p}{\partial x} - \rho \frac{\partial^2 u}{\partial t^2} = 0, \quad (4a)$$

$$\alpha \frac{\partial^2 u}{\partial x \partial t} - \frac{K_D}{g} \frac{\partial}{\partial x} \left(\frac{1}{\rho_f} \frac{\partial p}{\partial x} + \frac{\partial^2 u}{\partial t^2} \right) + \frac{1}{Q} \frac{\partial p}{\partial t} = 0, \quad (4b)$$

where $x = x_1$ and $M = \lambda + 2\mu$ is the oedometric modulus, being λ and μ the Lamé constants. According to one-dimensional context ($u_2 = 0, u_3 = 0$), it is also assumed that the displacement and pore pressure fields can be expressed as $u = u(x, t)$ and $p = p(x, t)$, so that their derivatives with respect to x_2 and x_3 vanish.

The set of equations for the one-dimensional wave propagation (4) can be reduced to a single equation as follows. The derivative of equation (4b) with respect to x yields

$$\alpha \frac{\partial^3 u}{\partial x^2 \partial t} - \frac{K_D}{g} \frac{\partial^2}{\partial x^2} \left(\frac{1}{\rho_f} \frac{\partial p}{\partial x} + \frac{\partial^2 u}{\partial t^2} \right) + \frac{1}{Q} \frac{\partial^2 p}{\partial t \partial x} = 0, \quad (5)$$

whereas from (4a), the following relation can be obtained

$$\frac{\partial p}{\partial x} = \frac{M}{\alpha} \frac{\partial^2 u}{\partial x^2} - \frac{\rho}{\alpha} \frac{\partial^2 u}{\partial t^2}, \quad (6)$$

which can be substituted into (5), in order to eliminate the dependence on the pore pressure, thus yielding the governing equation for the one-dimensional case in terms of the solid displacement field only

$$\frac{K_D}{\alpha g} \frac{\partial^2}{\partial x^2} \left[\left(\frac{\rho}{\rho_f} - \alpha \right) \frac{\partial^2 u}{\partial t^2} - \frac{M}{\rho_f} \frac{\partial^2 u}{\partial x^2} \right] + \frac{1}{\alpha} \frac{\partial}{\partial t} \left[\left(\alpha^2 + \frac{M}{Q} \right) \frac{\partial^2 u}{\partial x^2} - \frac{\rho}{Q} \frac{\partial^2 u}{\partial t^2} \right] = 0. \quad (7)$$

If we neglect the gradient of fluid inertial forces in equation (4b), namely neglecting the term $\partial^3 u / \partial x \partial t^2$, equation (7) reduces to

$$\frac{K_D}{\alpha g} \frac{\partial^2}{\partial x^2} \left[\frac{\rho}{\rho_f} \frac{\partial^2 u}{\partial t^2} - \frac{M}{\rho_f} \frac{\partial^2 u}{\partial x^2} \right] + \frac{1}{\alpha} \frac{\partial}{\partial t} \left[\left(\alpha^2 + \frac{M}{Q} \right) \frac{\partial^2 u}{\partial x^2} - \frac{\rho}{Q} \frac{\partial^2 u}{\partial t^2} \right] = 0. \quad (8)$$

Alternatively, if the term $\partial^3 u / \partial x \partial t^2$ is neglected in equation (4b), the following relation can be obtained from equation (4b):

$$\frac{\partial^2 u}{\partial x \partial t} = -\frac{1}{\alpha Q} \frac{\partial p}{\partial t} + \frac{K_D}{\alpha g \rho_f} \frac{\partial^2 p}{\partial x^2}. \quad (9)$$

This relation can be substituted in the derivative with respect to x and t of equation (4a) in order to eliminate the dependence on the solid displacement field, thus yielding the governing equation for the one-dimensional case in terms of the pore pressure field only

$$\frac{K_D}{\alpha g} \frac{\partial^2}{\partial x^2} \left(\frac{\rho}{\rho_f} \frac{\partial^2 p}{\partial t^2} - \frac{M}{\rho_f} \frac{\partial^2 p}{\partial x^2} \right) + \frac{1}{\alpha} \frac{\partial}{\partial t} \left[\left(\alpha^2 + \frac{M}{Q} \right) \frac{\partial^2 p}{\partial x^2} - \frac{\rho}{Q} \frac{\partial^2 p}{\partial t^2} \right] = 0. \quad (10)$$

It can be noted that this expression has the same structure of (8). The governing equations (8) and (10) can be easily solved if the solutions $u(x, t)$ and $p(x, t)$ are assumed to be

expressed in the following separation form

$$u(x, t) = X(x)T(t), \quad (11a)$$

$$p(x, t) = P(x)T(t), \quad (11b)$$

so that (8) and (10) can be rewritten as

$$\frac{K_D}{\alpha g} \left(\frac{\rho}{\rho_f} \frac{\partial^2 X}{\partial x^2} \frac{\partial^2 T}{\partial t^2} - \frac{M}{\rho_f} \frac{\partial^4 X}{\partial x^4} T \right) + \frac{1}{\alpha} \left[\left(\alpha^2 + \frac{M}{Q} \right) \frac{\partial^2 X}{\partial x^2} \frac{\partial T}{\partial t} - \frac{\rho}{Q} X \frac{\partial^3 T}{\partial t^3} \right] = 0, \quad (12a)$$

$$\frac{K_D}{\alpha g} \left(\frac{\rho}{\rho_f} \frac{\partial^2 P}{\partial x^2} \frac{\partial^2 T}{\partial t^2} - \frac{M}{\rho_f} \frac{\partial^4 P}{\partial x^4} T \right) + \frac{1}{\alpha} \left[\left(\alpha^2 + \frac{M}{Q} \right) \frac{\partial^2 P}{\partial x^2} \frac{\partial T}{\partial t} - \frac{\rho}{Q} P \frac{\partial^3 T}{\partial t^3} \right] = 0. \quad (12b)$$

respectively, where the explicit dependence on variables x and t of the functions X , P , and T is omitted. However, to obtain an effective separation of the variables, the following form for $X(x)$ and $P(x)$ should be employed:

$$X(x) = C_1 \cos(\xi x) + C_2 \sin(\xi x), \quad (13a)$$

$$P(x) = C_3 \cos(\xi x) + C_4 \sin(\xi x), \quad (13b)$$

namely, the same value ξ is assumed for solid and fluid phases, which holds true for boundary conditions involving the same Fourier expansion for solid and fluid displacements. In this way, equations (12) can be rewritten as

$$\frac{\partial^3 T}{\partial t^3} + a_1 \xi^2 \frac{\partial^2 T}{\partial t^2} + a_2 \xi^2 \frac{\partial T}{\partial t} + a_3 \xi^4 T = 0, \quad (14)$$

where

$$a_1 = \frac{K_D Q}{\rho g} \frac{\rho}{\rho_f}, \quad (15a)$$

$$a_2 = \frac{Q}{\rho} \left(\alpha^2 + \frac{M}{Q} \right), \quad (15b)$$

$$a_3 = \frac{K_D Q M}{\rho_f \rho g}. \quad (15c)$$

The general solution of (14) is

$$T(t) = e^{\psi t}, \quad (16)$$

so that the characteristic equation associated to (14) is

$$\psi^3 + a_1 \xi^2 \psi^2 + a_2 \xi^2 \psi + a_3 \xi^4 = 0. \quad (17)$$

One real root and two complex conjugate roots are the solutions of the characteristic equation, corresponding to the propagation of one single longitudinal wave. Therefore, the general solution has the form

$$u(x, t) = [C_1 \cos(\xi x) + C_2 \sin(\xi x)] \left[e^{\psi_1 t} (C_5 \cos(\eta t) + C_6 \sin(\eta t)) + C_7 e^{\psi_2 t} \right], \quad (18a)$$

$$p(x, t) = [C_3 \cos(\xi x) + C_4 \sin(\xi x)] \left[e^{\psi_1 t} (C_8 \cos(\eta t) + C_9 \sin(\eta t)) + C_{10} e^{\psi_2 t} \right], \quad (18b)$$

where the velocity of propagation of the longitudinal wave is given by $V = \eta/\xi$. The existence of one single longitudinal wave is obviously in contrast with Biot's equations, in which the propagation of two longitudinal waves is predicted within the range of high permeabilities or short propagation lengths. Moreover, the existence of one single longitudinal wave as evaluated from u - p formulation is in contrast with numerical findings by Han et al. [33].

The constants C_i ($i = 1, \dots, 4$) and ξ can be determined by imposing the boundary conditions, whereas the constants C_i ($i = 5, \dots, 10$) and η can be determined by imposing the initial conditions. The imposition of the initial and of the boundary conditions for the determination of the analytical solution is provided for the case study in section 3.1.

Two extreme cases may potentially occur and are discussed below. In the limit of very low permeability ($K_D \rightarrow 0$), equation (9) reduces to

$$p = -\alpha Q \frac{\partial u}{\partial x}, \quad (19)$$

and substituting this expression into equation (4a) leads to

$$(M + \alpha^2 Q) \frac{\partial^2 u}{\partial x^2} - \rho \frac{\partial^2 u}{\partial t^2} = 0, \quad (20)$$

which represents the equation of one longitudinal wave propagating with velocity equal to

$$V_c = \sqrt{\frac{M + \alpha^2 Q}{\rho}}. \quad (21)$$

It is worth noting that this velocity coincides with Biot's results for very low permeability.

In the limit of very high permeability ($K_D \rightarrow +\infty$), equation (8) reduces to

$$\frac{\rho}{\rho_f} \frac{\partial^4 u}{\partial x^2 \partial t^2} - \frac{M}{\rho_f} \frac{\partial^4 u}{\partial x^4} = 0, \quad (22)$$

which is equivalent to

$$M \frac{\partial^2 u}{\partial x^2} - \rho \frac{\partial^2 u}{\partial t^2} = 0, \quad (23)$$

representing the equation of one longitudinal wave propagating with velocity equal to $V = \sqrt{M/\rho}$. This velocity is much smaller than that obtained by Biot for very high permeability and has no physical meaning. It is worth recalling that the analytical solution described above has been obtained by neglecting the gradient of fluid inertial forces $\partial^3 u / \partial x \partial t^2$ in equation (4b).

2.2 Implementation of the u - p formulation

The u - p formulation is implemented as a user-defined, 2D, finite element (through a UEL subroutine) in the commercial finite element code Abaqus Unified FEA®. In order to extend further the comparison between different formulations, two types of implementation of the u - p formulation are performed: in the first one, the gradient of pore fluid inertial forces in the mass balance equation (1e) are neglected, and in the second one, these forces are taken into account. In both implementation types, eight node finite elements are used for the discretisation of the solid displacements, whereas four node elements are

Table 1: Material properties of the components of the two-phase medium. Properties referred to the solid phase and to the fluid phase are denoted with subscripts “s” and “f” respectively.

Parameter	Symbol	Value
Density	ρ	2020 kg m^{-3}
Porosity	n	0.4
Young modulus	E	1200 MPa
Poisson ratio	ν	0.3
Bulk modulus	K_s	$+\infty$
Solid phase density	ρ_s	2700 kg m^{-3}
Bulk modulus	K_f	2.1771 GPa
Fluid density	ρ_f	1000 kg m^{-3}

used for the pore pressure. The Hilber-Hughes-Taylor time integration implicit operator is employed in Abaqus simulations, which introduces numerical damping. According to Abaqus Unified FEA® manual, the following parameters for the Hilber-Hughes-Taylor integrator were chosen: $\alpha = -0.06$, $\beta = 0.28$, and $\gamma = 0.56$. Volumetric-locking effects were not detected in the simulations, so that no stabilizing scheme was needed in the UEL subroutine.

2.3 u - U formulation and its implementation

The governing equations for the u - U formulation within the small strain framework are given by [21, 30, 34]

$$\mathbb{D}_{ijkl}\varepsilon_{kl} + (\alpha - n)^2 Q \frac{\partial \varepsilon_{jj}}{\partial x_i} + n(\alpha - n) Q \frac{\partial^2 U_j}{\partial x_j \partial x_i} + (1 - n)\rho_s g_i - (1 - n)\rho_s \frac{\partial^2 u_i}{\partial t^2} - \rho_a \left(\frac{\partial^2 u_i}{\partial t^2} - \frac{\partial^2 U_i}{\partial t^2} \right) - \frac{n^2}{k} \left(\frac{\partial u_i}{\partial t} - \frac{\partial U_i}{\partial t} \right) = 0, \quad (24a)$$

$$n(\alpha - n) Q \frac{\partial \varepsilon_{jj}}{\partial x_i} + n^2 Q \frac{\partial^2 U_j}{\partial x_j \partial x_i} + n\rho_f g_i - n\rho_f \frac{\partial^2 U_i}{\partial t^2} - \rho_a \left(\frac{\partial^2 U_i}{\partial t^2} - \frac{\partial^2 u_i}{\partial t^2} \right) - \frac{n^2}{k} \left(\frac{\partial U_i}{\partial t} - \frac{\partial u_i}{\partial t} \right) = 0, \quad (24b)$$

where U_i is the absolute displacement of the pore fluid, ρ_a is the added mass of pore fluid (which is neglected here for the sake of consistency with u - p formulation), and ρ_s is the density of the solid constituent. The u - U formulation is implemented in an in-house 1D FEM code [30], in which both the solid and the pore fluid displacements are approximated with quadratic elements. The numerical solution proved to be consistent with the analytical solution of Biot’s equations proposed by Gajo & Mongiovi [31] and no volumetric-locking problem was detected in the simulations performed for this study, so that no stabilizing scheme was needed in the implementation of the numerical code. Numerical damping is introduced in the Newmark scheme, assuming the parameters $\alpha = 0.28$ and $\beta = 0.56$ that are in agreement with the u - p formulation implementation strategy.

3 The case studies

This section presents two case studies on the transient response of a finite length, saturated soil column subjected to a longitudinal dynamic excitation. The first case study is representative of the typical wave propagation occurring in specimens during dynamic tests performed in a laboratory, whereas the second case study is related to real earthquakes (in the case of a near-field or epicentral area) and has a potential impact on Geotechnical Earthquake Engineering. The soil column is modelled as a water-saturated, linear elastic isotropic porous material, whose properties are summarised in table 1, and both u - p and u - U formulations are employed. The soil column is laterally constrained, so that lateral displacements and horizontal strains are equal to zero. No water flux is permitted through the lateral boundaries. The response of the system is thought of as an incremental response, therefore gravity is neglected and null initial stress state and null pore pressure are assumed.

3.1 Analytical solution and computational model for the first case study

3.1.1 Determination of the analytical solution

In the first case study, the analytical solution has been applied to a soil column with length $L = 0.08$ m and constrained at the top and bottom surfaces. The initial pore pressure is assumed equal to zero and null water flux is assumed at both top and bottom surfaces of the sample, which is initially undeformed. The initial condition of the sample consists in a rigid longitudinal displacement $u(x, 0) = -0.1 \mu\text{m}$. A step variation of the longitudinal displacement equal to $0.1 \mu\text{m}$ is then applied simultaneously at the top and bottom surfaces, thus the final displacement at the top and bottom ends is null. This means that the sample is initially shifted by a limited amount ($u(x, 0) = -0.1 \mu\text{m}$) with respect to the reference system while keeping the sample undeformed and at rest. The prescribed displacement variation generates two longitudinal waves in the soil column propagating from the top and bottom boundaries, respectively. To obtain the analytical solution, the following initial conditions need to be imposed

$$\begin{aligned} u(x, 0) &= f(x) = -0.1 \mu\text{m}, & \left. \frac{\partial u}{\partial t} \right|_{t=0} &= 0 \text{ m s}^{-1}, \\ p(x, 0) &= g(x) = 0 \text{ Pa}, & \left. \frac{\partial p}{\partial t} \right|_{t=0} &= 0 \text{ Pa s}^{-1}, \end{aligned} \quad (25)$$

together with the following boundary conditions applied at the top and at the bottom of the sample

$$u(0, t) = h(t), \quad u(L, t) = h(t). \quad (26)$$

where $h(t)$ is the Heaviside step function modified as follows

$$h(t) = \begin{cases} -0.1 \mu\text{m}, & \text{for } t < 0 \text{ s}, \\ 0 \text{ m}, & \text{for } t \geq 0 \text{ s}. \end{cases} \quad (27)$$

In this way, summation of $0.1 \mu\text{m}$ to $u(x, t)$ leads to a solution with a clear physical meaning. The boundary conditions allow to determine the integration constants $C_1, C_3,$

and ξ , so that the general solution (18) can be written as

$$u(x, t) = \left[e^{\psi_1 t} (C_5 \cos(\eta t) + C_6 \sin(\eta t)) + C_7 e^{\psi_2 t} \right] \sin \frac{m\pi x}{L}, \quad (28a)$$

$$p(x, t) = \left[e^{\psi_1 t} (C_8 \cos(\eta t) + C_9 \sin(\eta t)) + C_{10} e^{\psi_2 t} \right] \cos \frac{m\pi x}{L}, \quad (28b)$$

where m is an integer. Imposition of the initial conditions allows for the determination of the 3+3 unknown coefficients C_i ($i = 5, \dots, 10$). In addition to the 2+2 initial conditions (25), 1+1 further conditions are obtained from equations (4a) and (4b), written for $t = 0$ and neglecting the term $\partial^3 u / \partial x \partial t^2$.

It is worth noting that the initial conditions for the solid displacements and pore pressures, $u(x, 0)$ and $p(x, 0)$, become a half-range expansion of $f(x)$ and $g(x)$, respectively, namely the Fourier sine and cosine series of $f(x)$ and $g(x)$, respectively. This strategy allows to have both effective stress σ''_{ij} and pore pressure p expressed by the same Fourier cosine series. The functions $f(x)$ and $g(x)$, herein considered, and their derivatives satisfy the conditions of continuity, which are sufficient to ensure the convergence of the Fourier series in $t = 0$. The convergence of the Fourier series for $t > 0$ has been always found, except for few cases where a steady oscillation occurred; in such cases, the mean value of the series has been selected.

In order to improve the comparison between the results obtained with the theoretical solution and those obtained from the numerical models, the step displacement boundary condition is replaced with a time-dependent displacement represented by a bi-linear function of time (represented in figure 1c and described in detail in the next subsection). In this case, the theoretical solution is obtained through a convolution integral of the analytical solution for the step displacement boundary condition.

3.1.2 Setup of the computational model

The setup of the computational model for the first case study is the following. The u - p formulation is implemented as a user-defined subroutine employed in Abaqus Unified FEA®, whereas the u - U formulation is implemented in an in-house FEM code.

Due to the choice of the setup described above, it can be noted that the system and its dynamic response are symmetric, so that in the numerical computations only half of the sample (with length $L/2 = 0.04$ m) can be modelled. In the reduced domain for the numerical computations (the upper half of the sample) employed for the u - p and the u - U formulations, only one wave propagates downwards and the following boundary conditions need to be imposed at the symmetry plane of the system: null displacement and no water flux, as illustrated in figure 1a (the bottom line). The loading is assigned by means of the following boundary condition (represented in figure 1c)

$$u(0, t) = \begin{cases} (0.5 \text{ m s}^{-1}) t, & \text{for } 0 \leq t < 0.2 \mu\text{s}, \\ 0.1 \mu\text{m}, & \text{for } t \geq 0.2 \mu\text{s}, \end{cases} \quad (29)$$

so that the time-dependent displacement is imposed only at the top surface of the sample, as shown in figure 1a.

The system is discretised with 800 elements, the total time of the simulation is equal to $15 \mu\text{s}$ and the time step is chosen equal to 2.5 ns . The analytical solution of Biot's

equations proposed in [31] is not shown here because it coincides with the numerical results of u - U formulation.

3.2 Computational model for the second case study

In the second case study, the soil column has a length of 15 m and is discretised with 30 elements; the top surface of the soil column is free, and the fluid pressure is equal to zero, as shown in figure 1b. A prescribed longitudinal displacement is applied at the bottom surface, which represents the vertical component of a real earthquakes, as shown in figure 1d. No water flux is allowed at the bottom and at the lateral surfaces; as a result, the bottom surface represents the contact with an impervious bedrock. A parametric study is performed by considering different permeability and porosity levels, different length of the soil column (i.e. different depth of the bedrock, always keeping the element size constant), and different ground motions. In particular, the Christchurch earthquake (2011, New Zealand) [33] is considered in the first set of simulations, then three additional real earthquakes data are employed to investigate the response of the u - p and of the u - U formulations, namely the earthquakes of L'Aquila (2009, Italy), Emilia (2012, Italy), and Norcia (2016, Italy) [8]. The time step of the simulation is chosen equal to 1×10^{-4} s. This value provides a good compromise between the computing time required by each numerical simulation and the accuracy of the solution. In fact, since every real earthquake data is composed of a broad range of frequencies (which can be evaluated by means of a Fourier analysis), it is necessary to employ a time step that allows to accurately capture the behaviour of most of these frequencies, and it is well known that this choice is related also to the element size employed for the domain discretisation and to the wave velocity. In particular, according to well known literature, at least 10 elements per wave length should be used to accurately capture the behaviour of a wave, so that Fourier analysis helps to determine the minimum element length of the finite element since it provides the maximum relevant frequency of the ground motion input, and hence the wave length. For instance, for a wave velocity of 1869.26 m s^{-1} (from the parameters described in table 1) having a relevant frequency up to 40 Hz (as illustrated in 1g for the Christchurch earthquake) the wave length is slightly smaller than 50 m, so that a spatial discretisation with elements having length of 0.5 m can be considered appropriate to accurately describe the behaviour of the ground motion and also possible effects of higher frequencies input. Similar checks were performed prior to analyse the other real earthquakes described in the manuscript. Therefore, for the numerical examples illustrated in this paper, the influence of the chosen mesh on the results revealed to be negligible. A further numerical investigation based on artificial signals (i.e. a sinusoid with different frequencies lying in the real earthquake frequency range, and the sum of a number of sinusoids), not reported for the sake of conciseness, was previously performed in order to identify a suitable range of time steps to employ in the simulations of real earthquakes. From these results, it has been drawn that in order to obtain an accurate solution for the proposed real earthquake data there is the need of a reduced time step with respect to common expectations [7, 33, 35–37]; the best accuracy level can be obtained with a time step equal to 1×10^{-5} s although the computing time is very high. A time step equal to 1×10^{-4} s produces solutions that are very close to those obtained by employing a time step equal to 1×10^{-5} s, and the computational cost is reduced. It is worth remarking that the time steps of $1 \times 10^{-5} \text{ s} \div 1 \times 10^{-4} \text{ s}$ are smaller than the time needed for the longitudinal wave

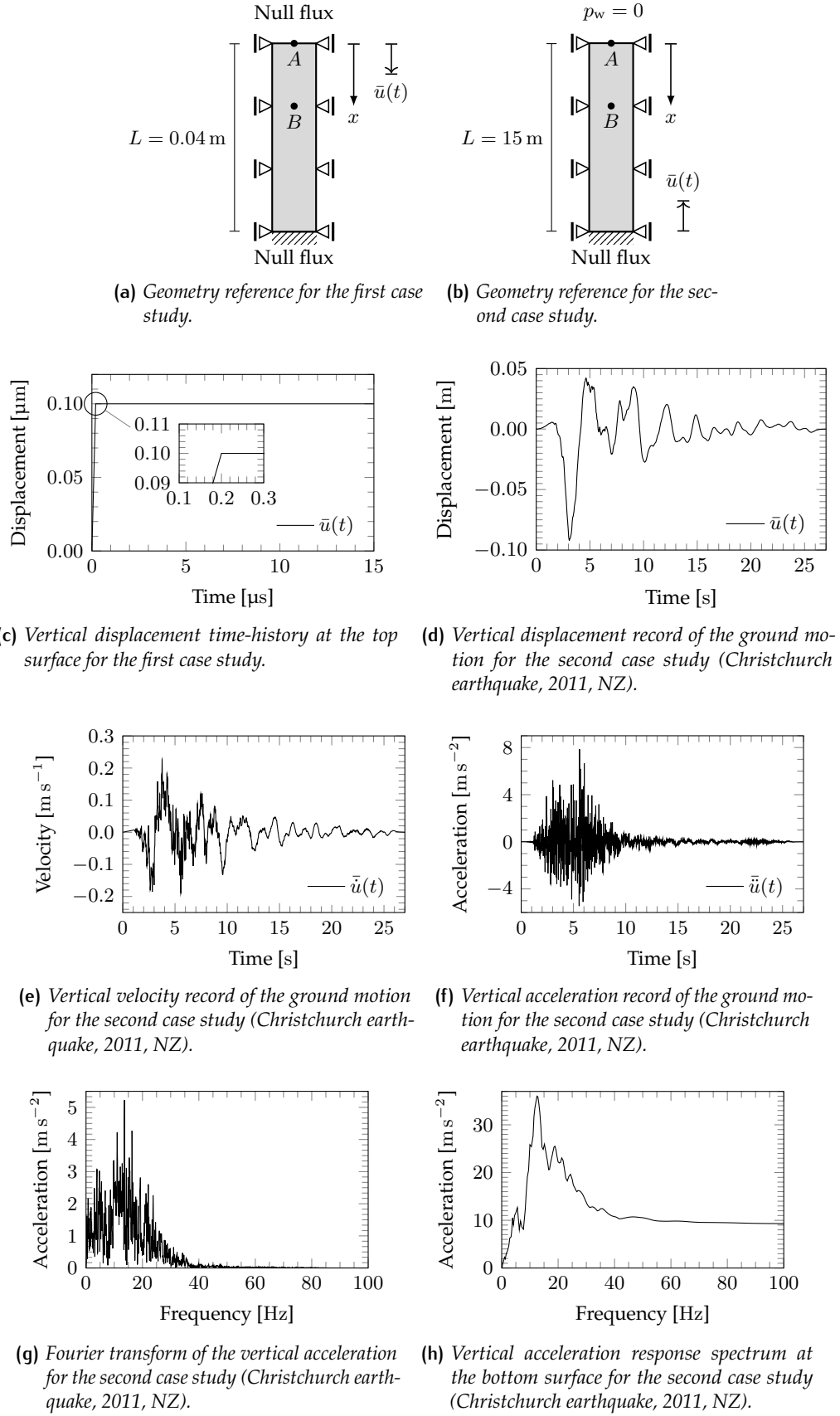


Figure 1: Reference schemes and loading time histories for the numerical simulations for the two case studies.

to travel the distance between two adjacent nodes (equal to 1.35×10^{-4} s) and are much smaller than the time step that could be deduced from the highest frequency of the input signal (40 Hz from figure 1g) according to Nyquist theorem (80 sampling points are much less than the 250 points that are employed in the simulation performed for this study).

A further effect is worth noting, which highlights the need of appropriate settings to perform accurate simulations when dealing with a wide range of frequency content of the imposed seismic ground motion. Abaqus introduces spurious oscillations when the time step of the simulation is two orders of magnitude smaller than the time step of the ground motion record (the manual suggests that for an implicit integration scheme a ratio higher than 20 already provides a certain level of accuracy). Also the in-house code for the $u-U$ formulation provides spurious oscillations, especially when the ratio between the ground motion record step and the integration time step is very high. A spline approximation of the input data (namely, the ground motion record in terms of displacement) was implemented in the in-house code for the $u-U$ formulation in order to eliminate spurious oscillations that arise from the employment of reduced time steps in the simulations. The time step provided for the spline approximation can be fixed a priori, so that a value of 5×10^{-4} s is selected for the in-house code for the $u-U$ formulation. In contrast, since the ground motions records employed in this study are provided with a time step equal to 5×10^{-3} s, spline approximation of the input is not needed in order to perform Abaqus simulations, as the ratio between the ground motion record time step and the simulation time step is equal to 50, which demonstrates to provide accurate results.

4 Results and discussion

This section is devoted to the analysis and the discussion of the results and their interpretation in terms of range of validity of the $u-p$ formulation (with and without fluid inertial terms) taking into account the water pore pressure and the vertical displacement and acceleration at different reference points. The first subsection summarises the results for the first case study, where the analytical solution is compared with numerical results obtained by employing the $u-U$ formulation. The results of the second case study, related to real earthquakes, are summarised in the second subsection: the novelty of investigating a frequency range of the imposed ground motion shows several features that are introduced and discussed.

4.1 First case study

In the first case study, the water pore pressure is measured at the reference point B (illustrated in figure 1a), which is 1 cm below the ground level. The results for the first case study are illustrated in figure 2 for different permeability levels. The results of the $u-p$ formulation are provided both for the cases in which the gradient of pore fluid inertial forces in the mass balance equation (1e) is neglected and is taken into account. These results of the $u-p$ formulation are compared with those obtained with the $u-U$ formulation that was validated against an analytical solution [31]. It can be observed that for large permeabilities ($K_D = 1 \times 10^{-5}$ m s⁻¹ in this case), the results obtained with $u-p$ formulation are completely unreliable, showing a sort of diffusion phenomenon. The amplitude of the pore pressure pulse evaluated with $u-p$ formulation is much smaller than

that evaluated with $u-U$ formulation. With the decrease of permeability, the results of $u-p$ formulation become closer to those of $u-U$ formulation, with the pore pressure tending to the form of a Dirac δ -function in the time domain. For permeabilities smaller than $K_D = 1 \times 10^{-8} \text{ m s}^{-1}$, the results are almost superposed to each other. It can be observed that pore fluid inertial forces in the mass balance equation are important in a range of permeabilities in which the $u-p$ formulation is not valid. It is worth noting that the above mentioned permeability values generally depend on the frequency content of the input signal, on the propagation length, and on the stiffness of the porous solid.

The numerical results of the $u-p$ formulation obtained without considering the pore fluid inertial forces in the mass balance equation (1e) are perfectly consistent with the analytical solution described in section 2.1.

4.2 Second case study

In the second case study, the water pore pressure is evaluated at the reference point B (illustrated in figures 1b), which is 5 m below the ground level, whereas the vertical displacement and acceleration are evaluated at the top of the soil column (point A in figure 1b). In addition to the analysis of the system response in the time domain (considered in terms of time history of acceleration and pore pressure), the response in the frequency domain is investigated in order to provide a detailed and comprehensive analysis of the effects of the frequency content of a real earthquake. Several numerical simulations are performed considering the four earthquakes described in section 3.2. The study includes a parametric analysis of the soil properties: in particular, the effects of the Young's modulus, of the porosity, and of the permeability are investigated by considering a soil layer with thickness equal to 15 m; furthermore, the parametric study includes also the case of a soil layer with thickness equal to 100 m. In order to provide a deeper insight in the analysis of the validity range of the $u-p$ formulation, the porosity and the Young's modulus are assumed to range from 0.1 to 0.8 and from 12 MPa to 1200 MPa respectively (which correspond to very extreme conditions that were mainly chosen to further explore and compare the response of the two formulations), whereas the investigated permeability levels range from $1 \times 10^{-6} \text{ m s}^{-1}$ to 1 m s^{-1} , thus including the behaviour of coarse to medium grained soils, i.e. from gravel and sand to medium silt. Each type of parametric study is performed for $u-U$ formulation and for the two versions of $u-p$ formulation (with and without the pore fluid inertia term). This means that a large number of simulations has been performed and therefore, for the sake of conciseness, only a limited number of detailed results is reported (figures 3-5). The results can be summarised in a compact form by employing the dimensionless chart provided by Zienkiewicz *et al.* [28, see their figure 3], as illustrated in figures 6 and 7, which highlight the limits of validity of $u-p$ formulation proposed by these authors [28]. This type of representation mainly refers to the validation of $u-p$ formulation in terms of frequency response.

It is worth recalling that, according to Zienkiewicz *et al.* [28, figure 3], zone (I) denotes the zone of slow phenomena; zone (II) and (III) denote, respectively, the zone of moderate speed and the zone of fast phenomena; zone (IV) (illustrated in figures 6 and 7 of this text) corresponds to the zone of undrained behaviour. In zone (I) and zone (IV), the employment of the $u-p$ formulation is admitted, as it provides a negligible difference with full Biot equation. Zone (II), which is highlighted with a hatch in figures 6 and 7 as well as in figure 3 of Zienkiewicz *et al.* [28], corresponds to a zone where the employment of

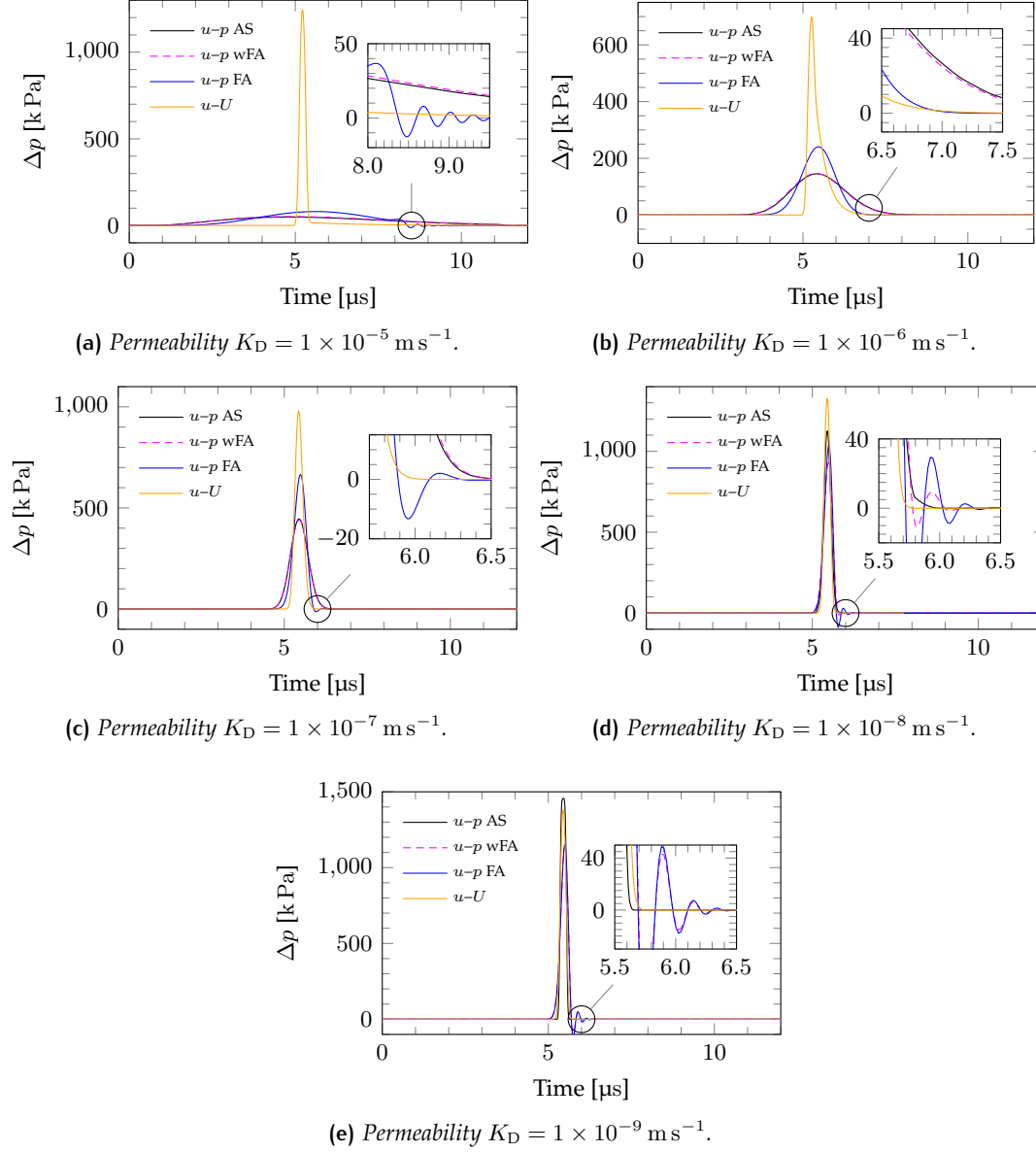


Figure 2: Comparison between $u-p$ and $u-U$ formulations for the first case study for different levels of permeability. Labels “FA” and “wFA” mean, respectively, with and without the gradient of fluid inertial force in the mass balance equation (1e), whereas “AS” denotes the analytical solution.

the $u-p$ formulation can be considered valid, although a limited difference is noted with respect to full Biot equation. This hatched area denotes the limits of applicability of $u-p$ formulation according to Zienkiewicz *et al.* [28]. In contrast, zone (III) corresponds to a zone where the $u-p$ formulation leads to unreliable results and only the full Biot equation is valid. In the present work, in addition to this graphical representation of the results, the error graphs in terms of ground acceleration at the ground surface and pore pressure at the depth of 5 m are provided for the different formulations as a function of different levels of soil layer thickness and soil properties, as illustrated in figures 8-10.

In order to provide a more comprehensive investigation, a comparison with previous results by Zienkiewicz *et al.* [28, figure 3] is performed by employing their dimensionless chart, which is based on the definition of two non-dimensional quantities Π_1 and Π_2 as:

$$\Pi_1 = \frac{K_D V_c^2}{g \beta \omega L^2} \quad (30a)$$

$$\Pi_2 = \frac{\omega^2 L^2}{V_c^2} \quad (30b)$$

where V_c is the compression wave velocity in the limit of low permeability defined by equation (21) (equal to 1869.26 m s^{-1} from the parameters described in table 1) and β is the ratio between the fluid density and the total density, whereas the definition of the angular frequency ω deserves a specific discussion as follows. It is important to remark that in the work of Zienkiewicz *et al.* [28] the loading is imposed at the ground surface as a sinusoid having angular frequency ω , so that this value is employed to evaluate the non-dimensional quantities Π_1 and Π_2 . In contrast, in this work the loading is imposed as a prescribed displacement at the base of the soil column that includes a wide range of angular frequencies (a representative condition of real earthquakes), so that the response of the system in terms of vertical displacement and acceleration is evaluated at the top of the soil column, and a representative value for ω must be chosen in order to evaluate Π_1 and Π_2 . Therefore, based on the modelling techniques and assumptions described in this section, the representative value of ω for the second case study is selected as the angular frequency associated with the largest acceleration amplitude in the Fourier series transform of the acceleration history at ground surface. This means that the value of ω depends on the formulation employed ($u-U$ or $u-p$, with or without pore fluid inertia terms), so that all the quantities involved in the evaluation of Π_1 and Π_2 are consistent. In the case of a prescribed ground motion that includes a wide frequency range, the angular frequency ω may also be chosen with different criteria. The shift of the simulation results shown in figures 6 and 7 (corresponding to different values of Π_1 and Π_2 for a specific level of permeability) is due to the change of the values of ω (defined above) when performing the Fourier analysis of the acceleration at the top of the soil column for different formulations. Therefore, a change of the definition of ω would lead to different values of Π_1 and Π_2 , but the difference between $u-U$ and $u-p$ formulation for the same level of permeability would remain unaltered. It is worth observing that the selected seismic input motions lead to data points laying along a nearly horizontal line in Zienkiewicz *et al.* [28]'s diagram and their location depends roughly only on permeability.

From figures 3-5 it can be observed that the results obtained with $u-p$ formulation and those obtained with $u-U$ formulation are different, but the difference decreases with decreasing levels of permeability, as highlighted in figures 8-10.

For instance, within the range of $K_D = 1 \times 10^{-1} \text{ m s}^{-1} \div 1 \times 10^0 \text{ m s}^{-1}$ the analysis of the vertical amplification and acceleration response spectrum obtained with $u-p$ and $u-U$ formulation are very different: in fact, the number of peaks and the frequency at which they occur are different. Only a very limited frequency range shows an error below 10% between $u-p$ and $u-U$ formulation. The response in terms of vertical acceleration and pore pressure over time are different and the error in their peaks can be above 20%.

For $K_D = 1 \times 10^{-3} \text{ m s}^{-1} \div 1 \times 10^{-2} \text{ m s}^{-1}$ the number of peaks shown in the acceleration amplification and response spectrum obtained with $u-p$ and $u-U$ formulation is the same, and the frequency at which they occur become closer to each other. The frequency range that shows an error below 10% between the two formulations is way larger than that obtained for the previous case. However, the behaviour in terms of vertical acceleration and pore pressure over time is still different, but the error in the estimation of the peak values is reduced, although it can still be above 15%.

Only with a lower value of permeability such as $K_D \leq 1 \times 10^{-4} \text{ m s}^{-1}$ the acceleration amplification and response spectrum obtained with different formulations become significantly closer to each other, leading to an error of the peak estimate that, approximately, does not exceed 5%. In this case, the response in terms of vertical acceleration and pore pressure over time becomes comparable and shows a limited error (around 5% for several time intervals and, in general, less than 10%) over the whole time domain. For such permeability range, it is possible to consider the results of the $u-p$ formulation (including the pore fluid inertial term) as a good approximation of the results provided by the $u-U$ formulation.

Within the range of permeabilities corresponding to those that are typical for fine sand and silt (i.e. $K_D = 1 \times 10^{-6} \text{ m s}^{-1} \div 1 \times 10^{-5} \text{ m s}^{-1}$) the response in both time and frequency domain of the $u-p$ and $u-U$ formulation can be considered the same: in fact, over these domains the solutions obtained with the two formulations cannot be distinguished, and only over very limited frequency intervals and time intervals show some differences, which are definitely lower than 5%.

From the results of the simulations for the second case study, it is apparent that the differences between $u-p$ and $u-U$ can be found simultaneously in the pore pressure, in the vertical acceleration, in the acceleration response spectrum, in the amplification factors, and in the frequency content. Furthermore, these differences tend to decrease as the permeability decreases, as it can be seen from figures 3-5, and become negligible only for permeabilities that are no greater than $1 \times 10^{-4} \text{ m s}^{-1}$. This permeability threshold holds true for all of the above mentioned relevant quantities (pore pressure, acceleration, acceleration response spectrum, amplification, and frequency content), so that this can be considered a more appropriate limit of validity of $u-p$ formulation with respect to $u-U$ formulation. The effects induced by neglecting the gradient of pore fluid inertial forces in the mass balance equation (1e) consist in a larger discrepancy with the results obtained by using the $u-U$ formulation, especially when the permeability is equal or greater than $1 \times 10^{-4} \text{ m s}^{-1}$. On the other hand, in the case of lower permeabilities, the gradient of pore fluid inertial forces has negligible effects, but this case corresponds to the permeability range where $u-p$ formulation can already be considered a good approximation of $u-U$ formulation.

According to Zienkiewicz *et al.* [28], the $u-p$ formulation would be expected to be unreliable for the selected seismic input motions for $K_D \geq 1 \times 10^{-1} \text{ m s}^{-1}$, whereas the error for $K_D \leq 1 \times 10^{-2} \text{ m s}^{-1}$ is limited, so that this can be considered within a reliability

zone, but this holds true for a ground motion input based on a single frequency. In contrast, according our investigation, when dealing with the frequency content of real earthquakes, the results reported in figures 3-5 and the results of the parametric analysis for the other real earthquakes (for different soil layer thickness and different levels of porosity and Young's modulus) clearly show that for $K_D = 1 \times 10^{-2} \text{ m s}^{-1}$ the differences in acceleration history, pore pressure, acceleration response spectrum, frequency content, and acceleration amplification are significant (6% to 20% for the acceleration and pore pressure peaks, above 50% for the acceleration amplification peak) and, therefore, the $u-p$ formulation cannot be considered reliable.

This means that the limits of applicability shown in figures 6 and 7 that were suggested by Zienkiewicz *et al.* [28] for the case of a single frequency loading may no longer hold true when dealing with an input ground motion that includes a wide range of frequencies. Therefore, the limits of applicability for a single frequency loading should be modified based on a thorough analysis of the results in terms of acceleration history, pore pressure, acceleration response spectrum, frequency content, and acceleration amplification, thus leading to modified boundaries of zone (II) in the (Π_1, Π_2) domain. The present study highlights this aspect: figures 6 and 7 show that the employment of the boundaries of zone (II) defined by Zienkiewicz *et al.* [28] may lead to wrong conclusions about the errors that can arise from the use of $u-p$ formulation in the case of a wide frequency range ground motion, so that these previous boundaries may be misleading. In particular, even if the set of points (Π_1, Π_2) representing the solutions provided in figures 6 and 7 obtained with $u-U$ and $u-p$ formulation for a given value of permeability and porosity may be almost coincident and may lie in the zone (II) (with the boundaries defined for a single frequency loading), this does not imply that the overall behaviour of the results obtained with $u-p$ formulation is a good approximation of the overall behaviour of the solutions obtained with $u-U$ formulation. For instance, this is apparent when considering the case of L'Aquila earthquake for a soil layer thickness equal to 100 m, porosity $n = 0.4$ and Young's modulus $E = 1200 \text{ MPa}$, as illustrated in figure 7d. When considering only this figure, according to the definition of zone (II) by Zienkiewicz *et al.* [28], it may be drawn that in the case of a permeability equal to $1 \times 10^{-2} \text{ m s}^{-1}$ the $u-p$ formulation is almost coincident with $u-U$ formulation. When considering also the other results in terms of acceleration history, pore pressure, acceleration response spectrum, frequency content, and acceleration amplification it is clear that this conclusion would not be correct: the error in the evaluation of the maximum acceleration and pore pressure ratios is still above 10%, as illustrated in figure 10.

As a consequence, the use of the sole original domain of Zienkiewicz *et al.* [28] should be made with caution when the input motion is composed of a wide range of frequencies and should be accompanied with other considerations about acceleration history, pore pressure, acceleration response spectrum, frequency content, and acceleration amplification, in order to verify the accuracy of the $u-p$ formulation; alternatively, starting from such in-depth analysis of all the features of the response of the system, it would be possible to modify the boundaries of zone (II) in the (Π_1, Π_2) domain for the frequency content of the real earthquake that a designer wants to investigate.

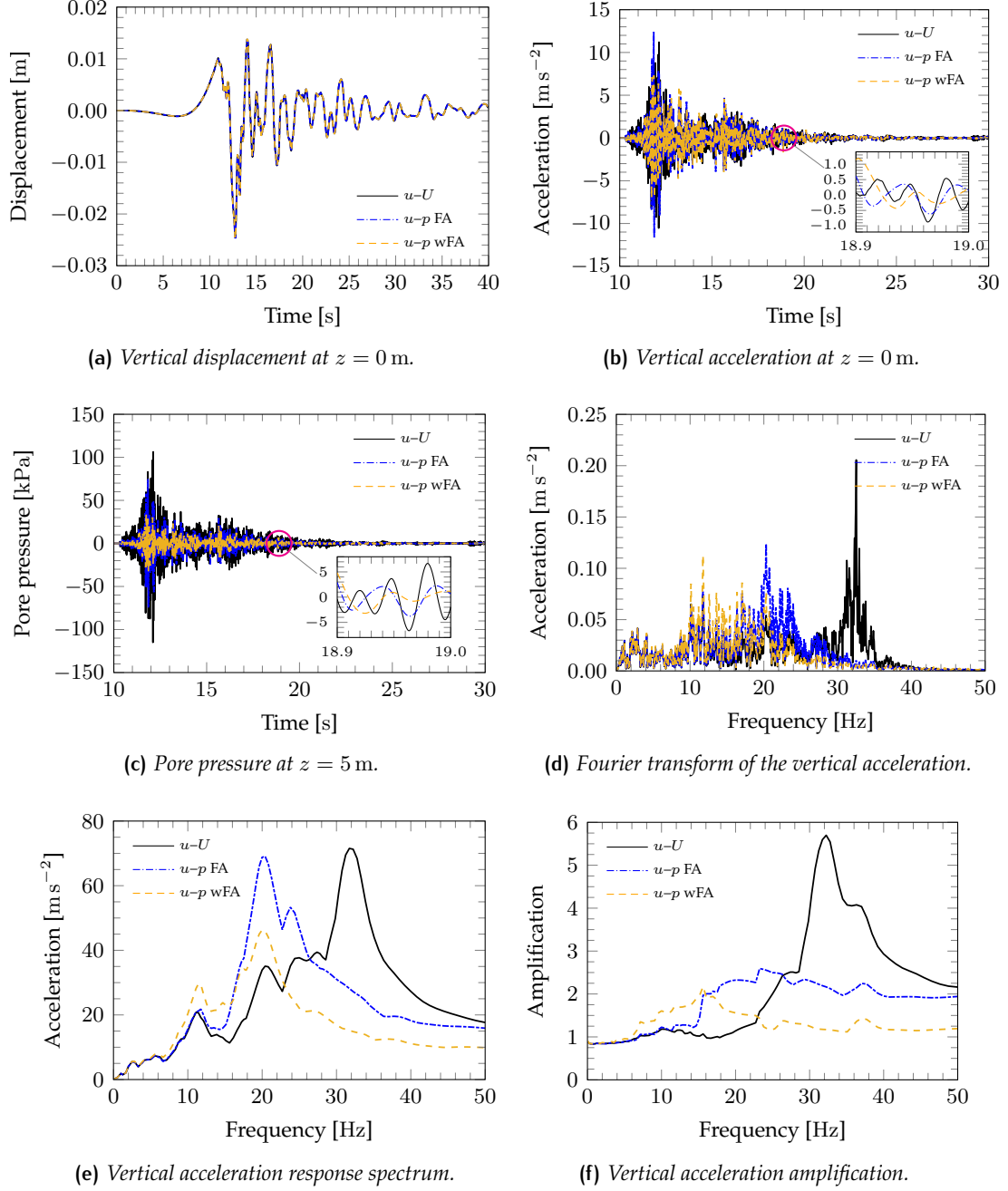


Figure 3: Comparison between $u-p$ and $u-U$ formulations for the L'Aquila earthquake assuming permeability $K_D = 1 \times 10^{-1} \text{ m s}^{-1}$, porosity $n = 0.4$, Young's modulus $E = 1200 \text{ MPa}$, and soil layer thickness $L = 15 \text{ m}$. Labels "FA" and "wFA" mean, respectively, with and without the gradient of fluid inertial force in the mass balance equation (1e).

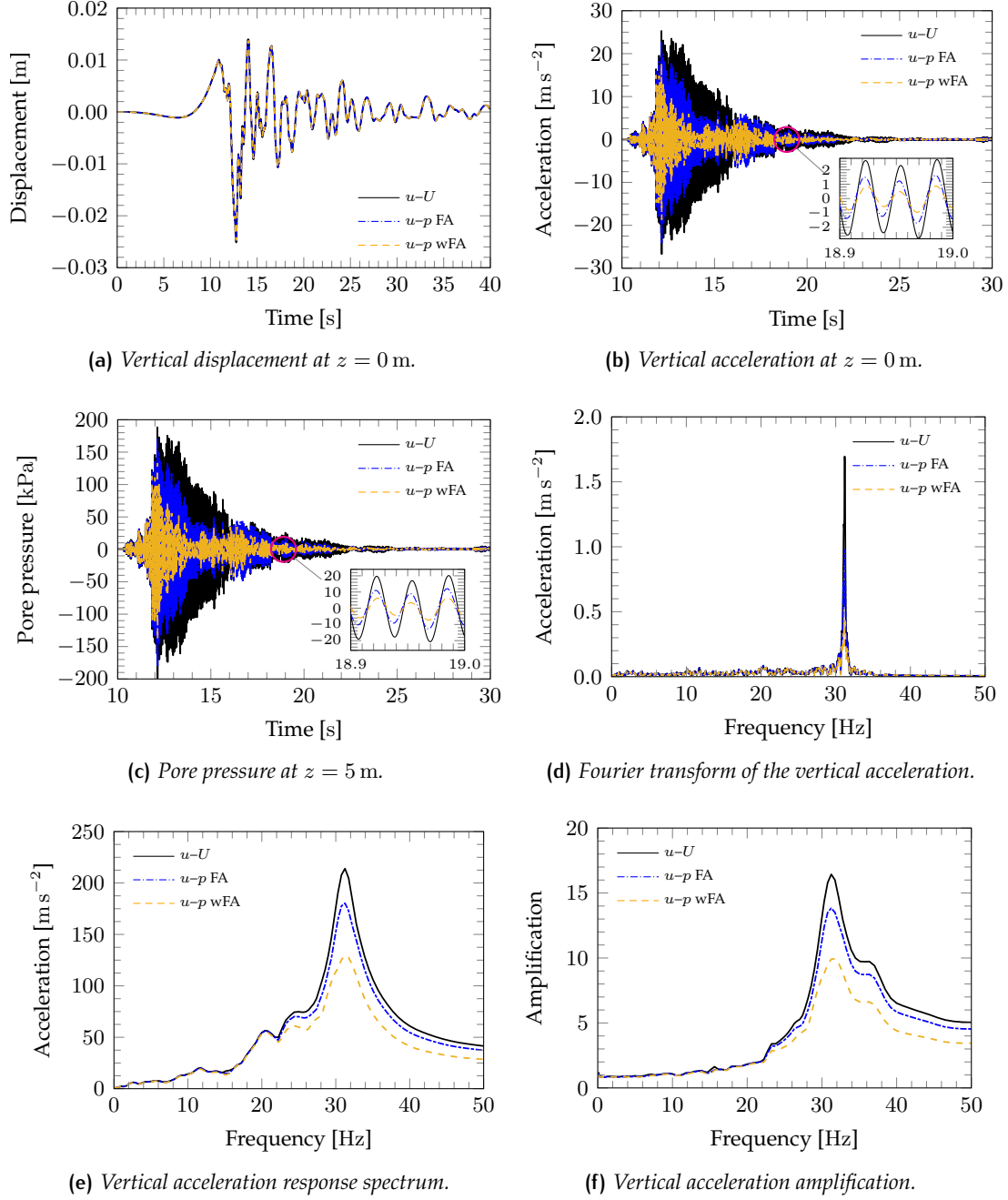


Figure 4: Comparison between $u-p$ and $u-U$ formulations for the L'Aquila earthquake assuming permeability $K_D = 1 \times 10^{-3} \text{ m s}^{-1}$, porosity $n = 0.4$, Young's modulus $E = 1200 \text{ MPa}$, and soil layer thickness $L = 15 \text{ m}$. Labels "FA" and "wFA" mean, respectively, with and without the gradient of fluid inertial force in the mass balance equation (1e).

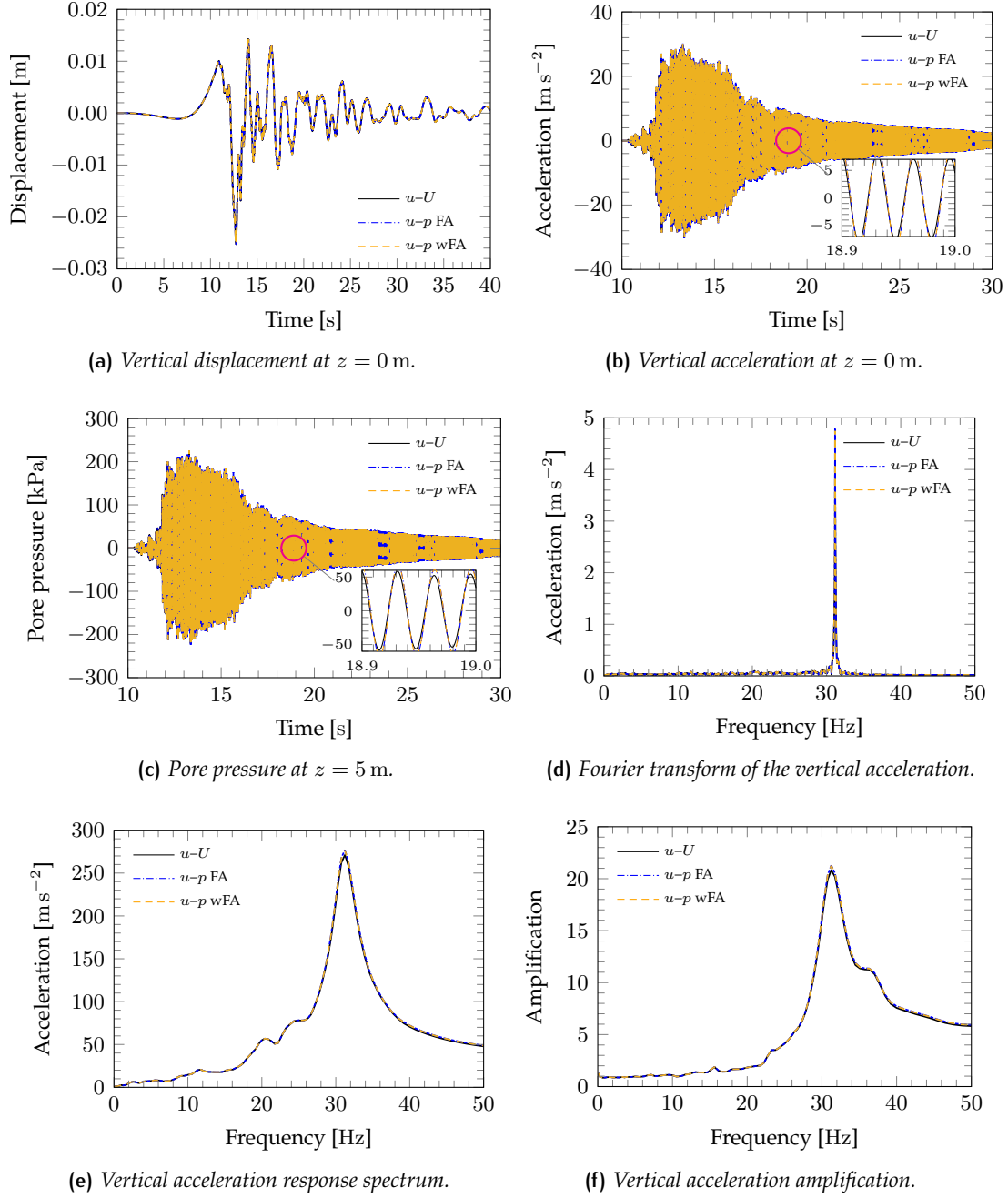


Figure 5: Comparison between $u-p$ and $u-U$ formulations for the L'Aquila earthquake assuming permeability $K_D = 1 \times 10^{-6} \text{ m s}^{-1}$, porosity $n = 0.4$, Young's modulus $E = 1200 \text{ MPa}$, and soil layer thickness $L = 15 \text{ m}$. Labels "FA" and "wFA" mean, respectively, with and without the gradient of fluid inertial force in the mass balance equation (1e).

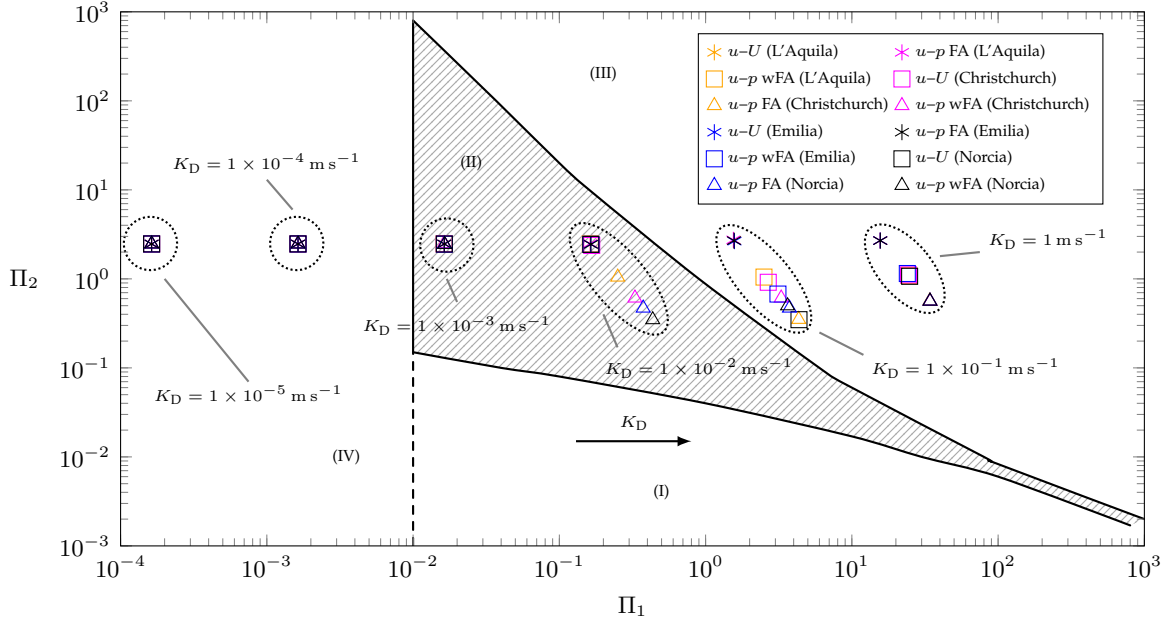


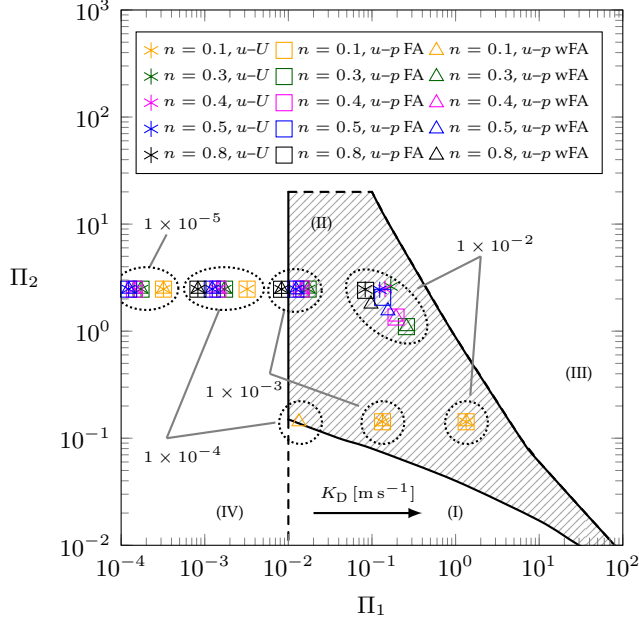
Figure 6: Comparison between $u-p$ and $u-U$ formulations in terms of the zones of applicability following Zienkiewicz *et al.* [28] for the four real earthquakes considered in section 3.2 in the case of $E = 1200 \text{ MPa}$, $n = 0.4$, and soil layer thickness equal to 15 m . According to their work, zone (I) denotes the zone of slow phenomena; zone (II) and (III) denote, respectively, the zone of moderate speed and the zone of fast phenomena; zone (IV) corresponds to the zone of undrained behaviour. Labels “FA” and “wFA” mean, respectively, with and without the gradient of fluid inertial force in the mass balance equation (1e).

5 Conclusions

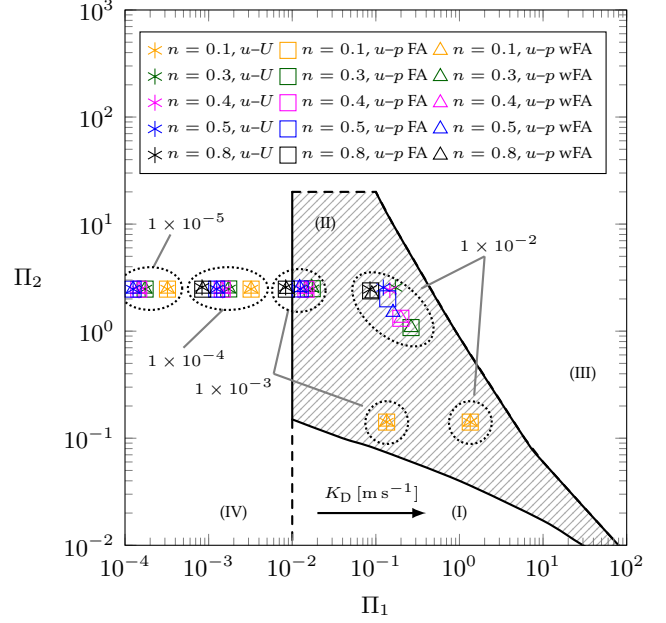
This article proposes two case studies on the transient response of a finite length, saturated soil column subjected to longitudinal dynamic excitation that are considered for the validation of $u-p$ formulation as compared to $u-U$ formulation. The analytical solution of the one-dimensional form of the $u-p$ formulation is derived for the problem of the propagation of a longitudinal wave. This solution is employed in the first case study as a benchmark in order to evaluate the permeability ranges in which $u-U$ and $u-p$ formulations can lead to the same results, as well as the estimate of the error of $u-p$ formulation with respect to $u-U$ formulation.

A second case study is analysed in order to determine the validity ranges of $u-p$ formulation in the context of the dynamic regime induced by a seismic ground motion, that embraces a large number of frequencies associated with different amplitudes.

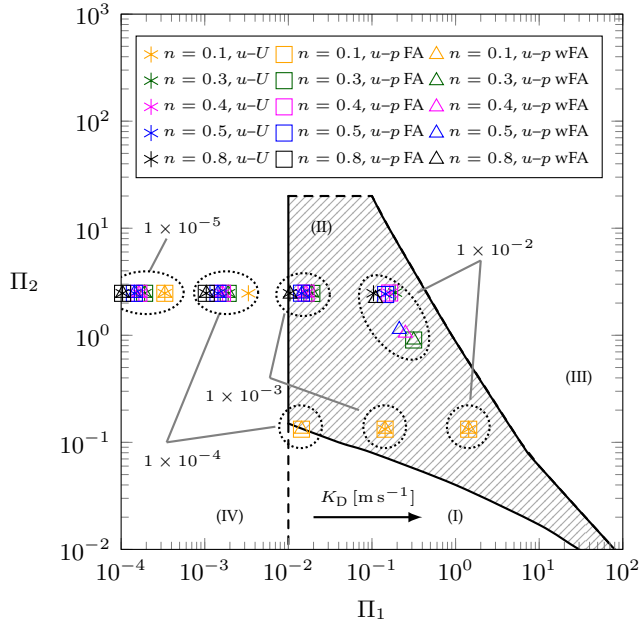
It is shown that the results for the second case study can lead to validity ranges that are slightly different from those identified by Zienkiewicz *et al.* [28] (which is valid for a single frequency ground motion): their dimensionless Π_1 – Π_2 domain needs to be updated based on a thorough analysis in terms of acceleration and pore pressure time history, acceleration response spectrum, frequency content and acceleration amplification for the case of a wide frequency range ground motion, so that the zone (II) reported in figures 6 and 7 (corresponding to that provided by Zienkiewicz *et al.* [28]) is converted to a newer one that denotes correctly the limits of applicability of $u-p$ formulation under real seismic actions.



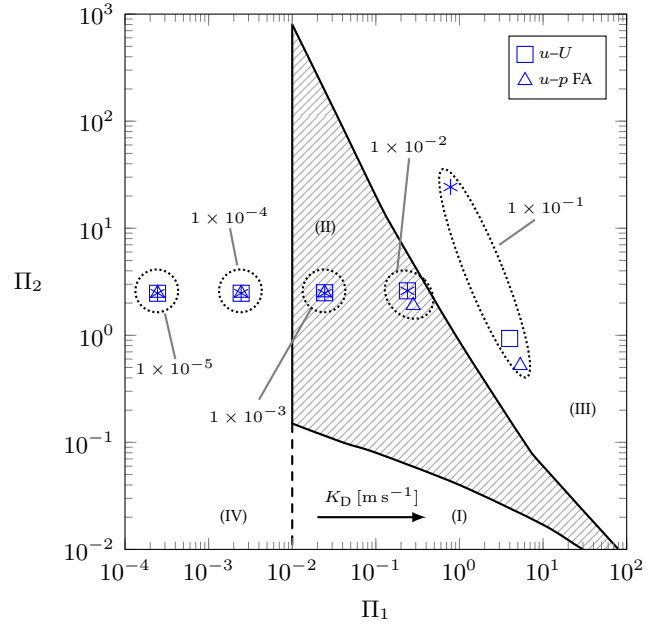
(a) $E = 12 \text{ MPa}$, $L = 15 \text{ m}$.



(b) $E = 120 \text{ MPa}$, $L = 15 \text{ m}$.

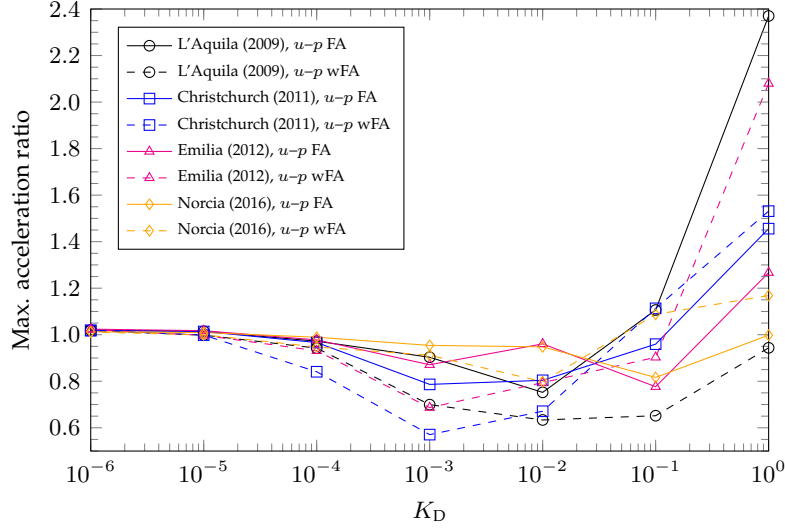


(c) $E = 1200 \text{ MPa}$, $L = 15 \text{ m}$.

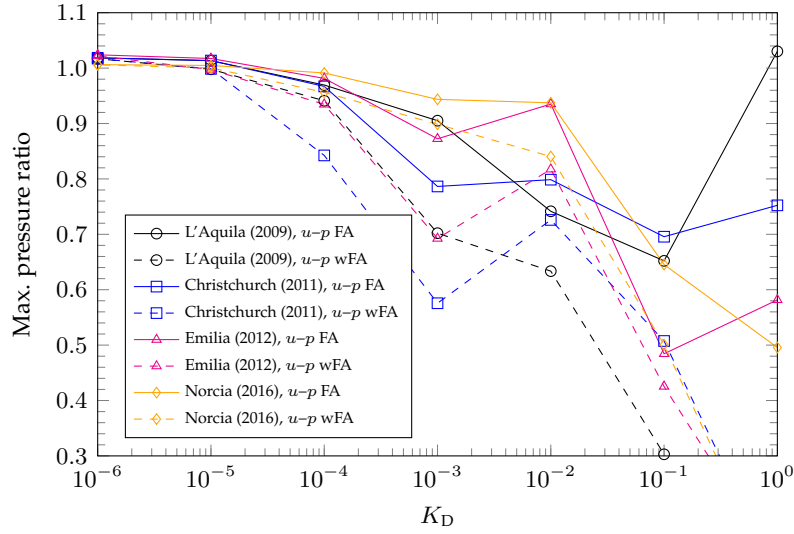


(d) $L = 100 \text{ m}$ with $E = 1200 \text{ MPa}$, $n = 0.4$.

Figure 7: Comparison between $u-p$ and $u-U$ formulations in terms of the zones of applicability following Zienkiewicz *et al.* [28] for the L'Aquila earthquake by employing a permeability range from $1 \times 10^{-5} \text{ m s}^{-1}$ to $1 \times 10^{-2} \text{ m s}^{-1}$ in subfigures (a)-(c) and from $1 \times 10^{-5} \text{ m s}^{-1}$ to $1 \times 10^{-1} \text{ m s}^{-1}$ in subfigure (d). Different levels of Young's modulus E , and different levels of permeability n are investigated for a soil layer thickness equal to 15 m. The effect of an increased soil thickness $L = 100 \text{ m}$ are investigated for $E = 1200 \text{ MPa}$ and $n = 0.4$. Labels "FA" and "wFA" mean, respectively, with and without the gradient of fluid inertial force in the mass balance equation (1e).

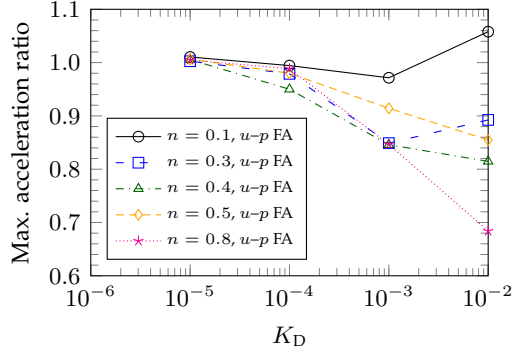


(a) Acceleration error as a function of permeability.

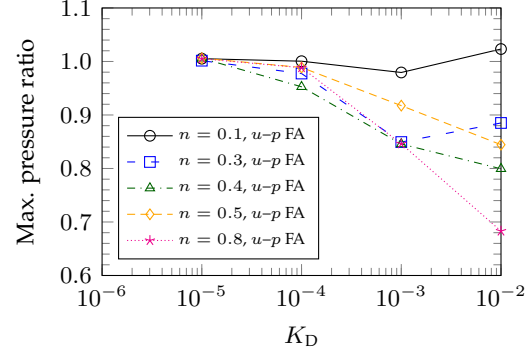


(b) Pore pressure error as a function of permeability.

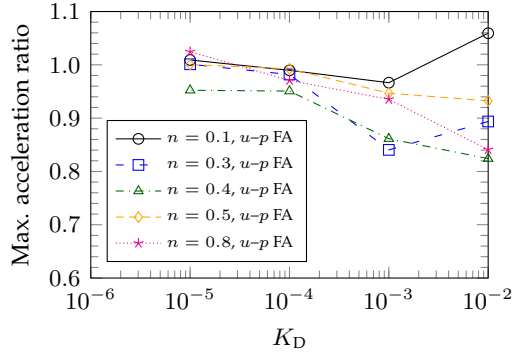
Figure 8: Comparison of the errors in the evaluation of the acceleration and pore pressure peaks for different levels of permeability for the four real earthquakes considered in section 3.2 in the case of $E = 1200 \text{ MPa}$, $n = 0.4$, and soil layer thickness equal to 15 m. The error is defined as the ratio between the acceleration peak computed using $u-p$ formulation (with and without the fluid inertial term) and the acceleration peak computed using $u-U$ formulation. Labels “FA” and “wFA” mean, respectively, with and without the gradient of fluid inertial force in the mass balance equation (1e).



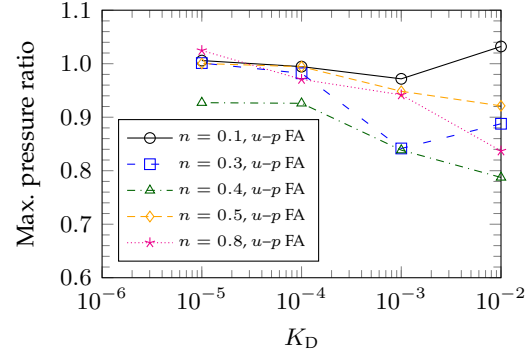
(a) Acceleration error as a function of porosity and permeability for $E = 12$ MPa.



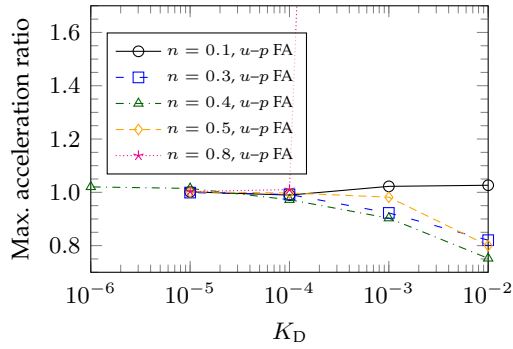
(b) Pore pressure error as a function of porosity and permeability for $E = 12$ MPa.



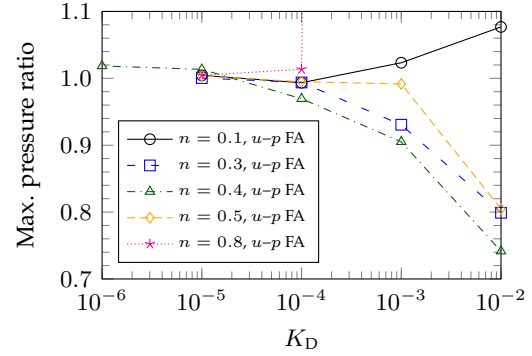
(c) Acceleration error as a function of porosity and permeability for $E = 120$ MPa.



(d) Pore pressure error as a function of porosity and permeability for $E = 120$ MPa.

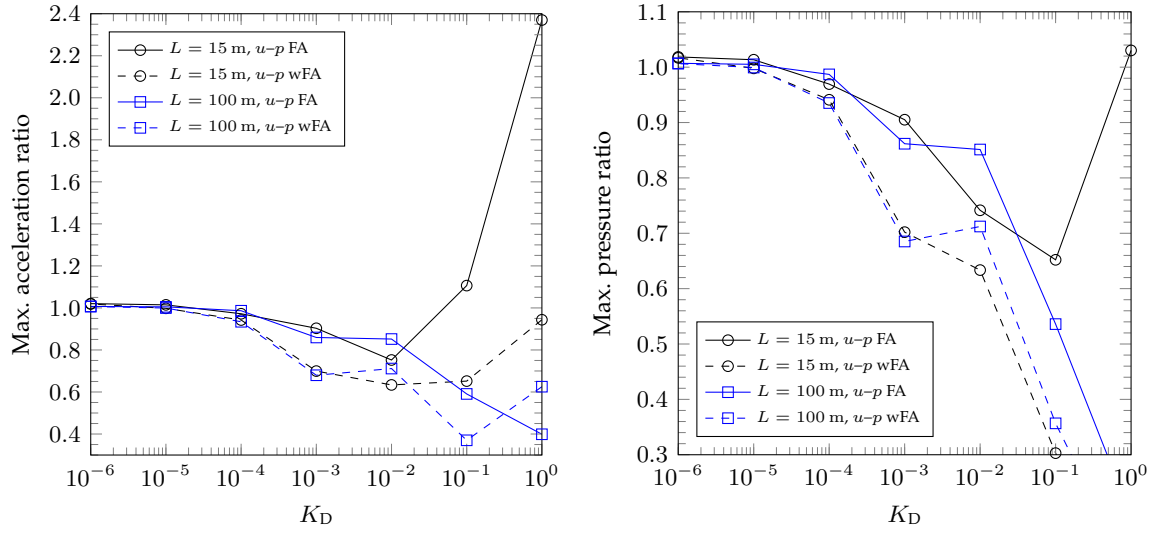


(e) Acceleration error as a function of porosity and permeability for $E = 1200$ MPa.



(f) Pore pressure error as a function of porosity and permeability for $E = 1200$ MPa.

Figure 9: Comparison of the errors in the evaluation of the acceleration and pore pressure peaks for different levels of porosity and Young's modulus for the L'Aquila earthquake for the case of soil layer thickness equal to 15 m. The error is defined as the ratio between the acceleration peak computed using $u-p$ formulation (with and without the gradient of fluid inertial force) and the acceleration peak computed using $u-U$ formulation. Label "FA" denotes that the gradient of fluid inertial force in the mass balance equation (1e) is taken into account.



(a) Acceleration error as a function of soil layer thickness and permeability. (b) Pore pressure error as a function of soil layer thickness and permeability.

Figure 10: Comparison of the errors in the evaluation of the acceleration and pore pressure peaks for different soil layer thickness for the L'Aquila earthquake in the case of $E = 1200$ MPa and $n = 0.4$. The error is defined as the ratio between the acceleration peak computed using $u-p$ formulation (with and without the gradient of fluid inertial force) and the acceleration peak computed using $u-U$ formulation. Labels "FA" and "wFA" mean, respectively, with and without the gradient of fluid inertial force in the mass balance equation (1e).

It is finally worth to remark that the proposed validity limits of $u-p$ formulation are limited to the linear elastic response of the soil and that non-linear soil response could affect the proposed limits of validity by increasing the discrepancies between the two formulations. Moreover, there is a strong dependency of dynamic soil response on the range of applied frequency and on propagation length: in fact, $u-p$ formulation provides reliable results for a permeability K_D smaller than $1 \times 10^{-4} \text{ m s}^{-1}$ for seismic ground motions (involving low frequencies and large propagation lengths), and for K_D smaller than $1 \times 10^{-8} \text{ m s}^{-1}$ for dynamic measurements in laboratory samples (typically involving very high frequencies and low propagation lengths).

Acknowledgements

This research has been supported by MIUR PON R&I 2014-2020 Program (project MITIGO, ARS01_00964). L.P.A. would like to thank the University of Trento for financial support and provision of excellent research facilities, and gratefully acknowledges resources, support, and research facilities from University of Liverpool (UK). A.G. gratefully acknowledges financial support from the EU Horizon 2020 research and innovation programme, grant agreement No 721816.

Data availability statement

The real earthquake waveforms employed as the input for the numerical simulations are openly available in ORFEUS Data Center at: www.orfeus-eu.org/data/strong/. All computational results are reproducible. All data, models, or code that support the findings of this study are available from the corresponding author upon reasonable request.

References

- [1] T. Larkin. "Seismic response of liquid storage tanks incorporating soil-structure interaction". In: *Journal of Geotechnical and Geoenvironmental Engineering, ASCE* 134.12 (2008), pp. 1804–1814. DOI: 10.1061/(ASCE)1090-0241(2008)134:12(1804) (cit. on p. 2).
- [2] G. Carta, A.B. Movchan, L.P. Argani, and O.S. Bursi. "Quasi-periodicity and multi-scale resonators for the reduction of seismic vibrations in fluid-solid systems". In: *Int. J. Eng. Sci.* 109 (2016), pp. 216–239. DOI: 10.1016/j.ijengsci.2016.09.010. URL: <https://arxiv.org/abs/1603.03652> (cit. on p. 2).
- [3] N.N. Ambraseys and J. Douglas. "Near-field horizontal and vertical earthquake ground motions". In: *Soil Dynamics and Earthquake Engineering* 23.1 (2003), pp. 1–18. DOI: 10.1016/S0267-7261(02)00153-7 (cit. on p. 2).
- [4] A. Elgamal and L.C. He. "Vertical earthquake ground motion records: An overview". In: *J. Earthq. Eng.* 8.5 (2004), pp. 663–697. DOI: 10.1016/S0267-7261(02)00153-7 (cit. on p. 2).
- [5] B. Shrestha. "Vertical ground motions and its effect on engineering structures: a state-of-the-art review". In: *Proceeding of International Seminar on Hazard Management for Sustainable Development in Kathmandu*. 29-30 November. Nepal, 2009, pp. 190–202 (cit. on p. 2).
- [6] S.J. Kim, C.J. Holub, and A.S. Elnashai. "Analytical Assessment of the Effect of Vertical Earthquake Motion on RC Bridge Piers". In: *Journal of Structural Engineering* 137.2 (2011), pp. 252–260. DOI: 10.1061/(ASCE)ST.1943-541X.0000306 (cit. on p. 2).
- [7] B. Han, L. Zdravković, S. Kontoe, and Taborda D.M.G. "Numerical investigation of the response of the Yele rockfill dam during the 2008 Wenchuan earthquake". In: *Soil Dyn. Earthq. Eng.* 88 (2016), pp. 124–142. DOI: 10.1016/j.soildyn.2016.06.002 (cit. on pp. 2, 11).
- [8] V. Bhanu, A.G. Özcebe, and C. Smerzini. "A study on vertical component of earthquake ground motion and its effect on a bridge". In: *Proceedings of the 16th European Conference on Earthquake Engineering* (June 18–21, 2018). Thessaloniki (Greece), 2018 (cit. on pp. 2, 11).
- [9] G.W. Housner and M.D. Trifunac. "Analysis of accelerograms - Parkfield earthquake". In: *Bull. Seism. Soc. Am.* 57.6 (1967), pp. 1193–1220. URL: <https://pubs.geoscienceworld.org/ssa/bssa/article-abstract/57/6/1193/101487/Analysis-of-accelerograms-Parkfield-earthquake?redirectedFrom=fulltext> (cit. on p. 2).
- [10] Y. Bozorgnia, M. Niazi, and K.W. Campbell. "Characteristics of Free-Field Vertical Ground Motion during the Northridge Earthquake". In: *Earthquake Spectra* 11.4 (1995), pp. 515–525. DOI: 10.1193/1.1585825 (cit. on p. 2).
- [11] N.A. Abramson and P.G. Somerville. "Effects of the hanging wall and footwall on ground motions recorded during the Northridge earthquake". In: *Bull. Seism. Soc. Am.* 86.1, Part B Suppl. (1996), S93–S99. URL: <https://pubs.geoscienceworld.org/ssa/bssa/article-abstract/86/1B/S93/120063/Effects-of-the-hanging-wall-and-footwall-on-ground?redirectedFrom=fulltext> (cit. on p. 2).
- [12] R. Teisseyre, M. Takeo, and E. Majewski. *Earthquake source asymmetry, structural media and rotation effects*. Ed. by R. Teisseyre, M. Takeo, and E. Majewski. 1st ed. Springer-Verlag Berlin Heidelberg, 2006. ISBN: 978-3-540-31336-6. DOI: 10.1007/3-540-31337-0 (cit. on p. 2).

- [13] S. Grimaz and P. Malisan. "Near field domain effects and their consideration in the international and Italian seismic codes". In: *Bollettino di Geofisica Teorica ed Applicata* 55.4 (2014), pp. 717–738. DOI: 10.4430/bgta0130 (cit. on p. 2).
- [14] A.J. Papazoglou and A.S. Elnashai. "Analytical and field evidence of the damaging effect of vertical earthquake ground motion". In: *Earthq. Eng. Struct. Dyn.* 25.10 (1996), pp. 1109–1137. DOI: 10.1002/(SICI)1096-9845(199610)25:10<1109::AID-EQE604>3.0.CO;2-0 (cit. on p. 2).
- [15] S.J. Kim and A.S. Elnashai. *Seismic assessment of RC structures considering vertical ground motion*. English. Report 08-03. Urbana-Champaign, USA: MAE Center, University of Illinois, 2008, pp. 1–274. URL: <http://mae.cee.illinois.edu/publications/reports/Report08-03.pdf> (cit. on p. 2).
- [16] L. Di Sarno, A.S. Elnashai, and Manfredi G. *Seismic response of RC members subjected to the 2009 L'Aquila (Italy) near-field earthquake ground motions*. English. Report 01-2010. Urbana-Champaign, USA: MAE Center, University of Illinois, 2010, pp. 1–48. URL: <http://www.reluis.it/images/stories/MAE%20Center%20Report%20-%20Di%20Sarno%20et%20al.pdf> (cit. on p. 2).
- [17] M.A. Biot. "Theory of propagation of elastic waves in a fluid-saturated porous solid. I. Low-frequency range". In: *J. Acoust. Soc. America* 28.2 (1956), pp. 168–178. DOI: 10.1121/1.1908239 (cit. on p. 2).
- [18] M.A. Biot. "Theory of propagation of elastic waves in a fluid-saturated porous solid. II. Higher Frequency Range". In: *J. Acoust. Soc. America* 28.2 (1956), pp. 179–191. DOI: 10.1121/1.1908241 (cit. on p. 2).
- [19] O.C. Zienkiewicz and T. Shiomi. "Dynamic behaviour of saturated porous media: the generalized Biot formulation and its numerical solution". In: *Int. J. Num. Anal. Geomech.* 8 (1984), pp. 71–96 (cit. on p. 2).
- [20] R. De Boer. *Theory of Porous Media: Highlights in Historical Development and Current State*. 1st ed. Berlin: Springer, 2000. ISBN: 978-3-642-64062-9. DOI: doi.org/10.1007/978-3-642-59637-7 (cit. on p. 2).
- [21] O.C. Zienkiewicz, A.H.C. Chan, M. Pastor, B.A. Schrefler, and A. Shiomi. *Computational Geomechanics with Special Reference to Earthquake Engineering*. New York, USA: John Wiley & Sons, 1999. ISBN: 0-471-98285-7 (cit. on pp. 2, 4, 8).
- [22] J.H. Prevost. "Nonlinear transient phenomena in saturated porous media". In: *Comput. Methods Appl. Mech. Eng.* 30.1 (1982), pp. 3–18. DOI: 10.1016/0045-7825(82)90052-4 (cit. on p. 2).
- [23] L. Monforte, P. Navas, J.M. Carbonell, M. Arroyo, and A. Gens. "Low order stabilized finite element for the full biot formulation in soil mechanics at finite strain". In: *Int. J. Numer. Anal. Methods. Geomech.* (2019), pp. 1–28. DOI: 10.1002/nag.2923 (cit. on p. 2).
- [24] P. Navas, M. Pastor, A. Yagüe, M.M. Stickley, D. Manzanal, and M. Molinos. "Fluid stabilization of the u-w Biot's formulation at large strain". In: *Int. J. Numer. Anal. Methods. Geomech.* (2020), pp. 1–17. DOI: 10.1002/nag.3158 (cit. on p. 2).
- [25] J.H. Prevost. "Wave propagation in fluid-saturated porous media: An efficient finite element procedure". In: *Int. J. Soil Dynam. Earthquake Eng.* 4.4 (1985), pp. 183–202. DOI: 10.1016/0261-7277(85)90038-5 (cit. on p. 2).
- [26] A. Gajo and R. Denzer. "Finite element modelling of saturated porous media at finite strains under dynamic conditions with compressible constituents". In: *Int. J. Numer. Meth. Engng.* 85.13 (2011), pp. 1705–1736. DOI: 10.1002/nme.3051 (cit. on p. 2).
- [27] B. Jeremić, Z. Cheng, M. Taiebat, and Dafalias Y. "Numerical simulation of fully saturated porous materials". In: *Int. J. Numer. Anal. Meth. Geomech.* 32.13 (2008), pp. 1635–1660. DOI: 10.1002/nag.687 (cit. on p. 2).

- [28] O.C. Zienkiewicz, C.T. Chang, and P. Bettess. "Drained, undrained, consolidating and dynamic behaviour assumptions in soils". In: *Géotechnique* 30.4 (1980), pp. 385–395. DOI: 10.1680/geot.1980.30.4.385 (cit. on pp. 2–4, 14, 16–18, 22, 23).
- [29] O.C. Zienkiewicz, A.H.C. Chan, M. Pastor, D.K. Paul, and T. Shiomi. "Static and dynamic behaviour of soils: a rational approach to quantitative solutions. I. Fully saturated problems". In: *Proc. Roy. Soc. A* 429.1877 (1990), pp. 285–309. DOI: 10.1098/rspa.1990.0061 (cit. on p. 2).
- [30] A. Gajo, A. Saetta, and R. Vitaliani. "Evaluation of three- and two-field finite element methods for the dynamic response of saturated soil". In: *Int. J. Numer. Meth. Eng.* 37.7 (1994), pp. 1231–1247. DOI: 10.1002/nme.1620370708 (cit. on pp. 3, 8).
- [31] A. Gajo and L. Mongiovì. "An analytical solution for the transient response of saturated linear elastic porous media". In: *Int. J. Numer. Anal. Meth. Geomech.* 19.6 (1995), pp. 399–413. DOI: 10.1002/nag.1610190603 (cit. on pp. 4, 8, 11, 13).
- [32] A. Nur and J.D. Byerlee. "An exact effective stress law for elastic deformation of rock with fluids". In: *J. Geophys. Res.* 76.26 (1971), pp. 6414–6419. DOI: 10.1029/JB076i026p06414 (cit. on p. 4).
- [33] B. Han, L. Zdravković, and S. Kontoe. "Analytical and numerical investigation of site response due to vertical ground motion". In: *Géotechnique* 68.6 (2018), pp. 467–480. DOI: 10.1680/jgeot.15.P.191 (cit. on pp. 7, 11).
- [34] A. Gajo. "The influence of viscous coupling in the propagation of elastic waves in saturated soil". In: *J. Geotech. Eng. - ASCE* 121.9 (1995), pp. 636–644. DOI: 10.1061/(ASCE)0733-9410(1995)121:9(636) (cit. on p. 8).
- [35] S. Kontoe, L. Zdravković, and D.M. Potts. "An assessment of time integration schemes for dynamic geotechnical problems". In: *Computers and Geotechnics* 35.2 (2008), pp. 253–264. DOI: 10.1016/j.compgeo.2007.05.001 (cit. on p. 11).
- [36] V. Tsaparli, S. Kontoe, D.M.G. Taborda, and D.M. Potts. "Numerical investigation of the effect of the irregular nature of seismic loading on the liquefaction resistance of saturated sand deposits". In: *SECED 2015 Conference: Earthquake Risk and Engineering towards a Resilient World*. 9-10 July. SECED. Cambridge, UK, 2015 (cit. on p. 11).
- [37] V. Tsaparli, S. Kontoe, D.M.G. Taborda, and D.M. Potts. "Vertical ground motion and its effects on liquefaction resistance of fully saturated sand deposits". In: *Proc. Roy. Soc. A* 472.2192 (2016), p. 20160434. DOI: 10.1098/rspa.2016.0434 (cit. on p. 11).